Journal of Manufacturing Processes 176 (2026) 892–908

Contents lists available at ScienceDirect

Journal of Manufacturing Processes

journal homepage: www.elsevier.com/locate/manpro

A novel hybrid mold design to enhance thermal efficiency of injection molding process

Vito BASILE [a,*], Giulia ZANIBONI [b], Riccardo PELACCIA [c], Rossella SURACE [a], Leonardo ORAZI [c], Francesco Giovanni MODICA [a], Irene FASSI [d]

[a] CNR-STIIMA, National Research Council, Institute of Industrial Intelligent Technologies and Systems for Advanced Manufacturing, via Paolo Lembo 38 F, 70124, Bari, Italy
[b] EN&TECH, University of Modena and Reggio Emilia, Piazzale Europa 1, 42124 Reggio Emilia, Italy
[c] DISMI, University of Modena and Reggio Emilia, Via Amendola 2, 42122, Reggio Emilia, Italy
[d] CNR-STIIMA, National Research Council, Institute of Industrial Intelligent Technologies and Systems for Advanced Manufacturing, via Alfonso Corti 12, 20133, Milan, Italy

ARTICLE INFO

Keywords:
Injection molding
Mold
Energy efficiency
Process sustainability
Process simulation

ABSTRACT

Optimizing energy consumption in injection molding is crucial for process sustainability, particularly in thermal energy management. This study presents an innovative hybrid mold design conceived to address three main drivers: 1) reducing the mold thermal-conductive mass; 2) introducing thermal insulation of the mold core; 3) reducing the mold weight. This novel concept, characterized by an optimized design with polymer structural components, was benchmarked against a conventional steel mold through transient thermal analyses under various initial conditions. Experimental and numerical analyses using COMSOL Multiphysics were performed to evaluate the thermal behavior of the molds during successive injection cycles. The numerical model demonstrated good predictive capability, with temperature deviations below 5 °C when compared with experimental measurements under different operating conditions. The results demonstrated that the hybrid molds significantly improved heat retention within the steel insert, achieving up to 50% higher steady-state temperatures, thereby reducing energy demand to maintain the desired thermal conditions. Furthermore, the sharply reduced thermal-conductive core mass shortens the duration of thermal transients, achieving higher thermal mold sensitivity. The feasibility of the injection molding with the novel hybrid mold was demonstrated. The deviations measured in the sample dimensions are in the range of (−2, −6)%, thus consistent with the nominal material shrinkage and the different thermal regimes. The achieved average weight reduction on support plates is about 88%, resulting in lower mechanical energy requirements for the opening/closing steps in molding cycles and facilitating mold handling during product turnover operations.

1. Introduction

Injection molding is the most widely recognized process for high-volume plastic and composite product manufacturing, due to its material versatility and geometric complexity [1]. However, it is also a significant energy-consuming process. In the context of growing demands for energy efficiency and sustainable manufacturing, optimizing the process, and in particular thermal aspects, has become of paramount importance [2,3].

A global assessment of energy consumption in injection molding reveals that total cycle time is the primary factor affecting overall energy usage, with cooling time representing the most significant part [4,5]. Therefore, reducing cooling time leads to a reduction of cycle time and energy consumption. This was also confirmed by a quantitative analysis of the mold cooling systems, highlighting the relevant mold design parameters to increase the effectiveness of the cooling and the overall energy efficiency of the process [6]. Thus, in traditional injection molding, properly managing the cooling phase becomes central to reducing energy consumption. A key strategy for this purpose is to optimize the thermal energy distribution within the mold [7,8]. For this

* Corresponding author.
E-mail addresses: vito.basile@cnr.it (V. BASILE), giulia.zaniboni@unimore.it (G. ZANIBONI), riccardo.pelaccia@unimore.it (R. PELACCIA), rossella.surace@cnr.it (R. SURACE), leonardo.orazi@unimore.it (L. ORAZI), francescogiovanni.modica@cnr.it (F.G. MODICA), irene.fassi@cnr.it (I. FASSI).

https://doi.org/10.1016/j.jmapro.2026.09.033
Received 20 January 2026; Received in revised form 13 August 2026; Accepted 14 September 2026
Available online 25 September 2026
1526-6125/© 2026 The Authors. Published by Elsevier Ltd on behalf of The Society of Manufacturing Engineers. This is an open access article under the CC BY license (http://creativecommons.org/licenses/by/4.0/).

purpose, the optimization of thermal energy transfer and harvesting in molds is required. Minimizing thermal energy dispersion means reducing heat loss to the environment and improving the overall thermal isolation of the mold system. The study of heat transfer within the mold and to the surrounding environment is of the utmost importance for minimizing energy waste. The thermal conductivity of mold materials significantly influences the system's thermal behavior. Therefore, optimization must address two main challenges: 1) Mold temperature control with high-efficiency heating and cooling; 2) minimizing thermal energy dispersion and waste.

Recently, some innovative methods were developed to process new materials, enhance equipment, improve product quality, increase productivity, reduce production costs, and minimize the environmental impact [1]. These studies remark on the importance of energy efficiency and the central relevance of molds (i.e., design, materials, precision) as the process's core component [2,3]. Hereafter, the current research and technology trends in the field are briefly discussed.

1.1. Variable mold temperature

A major research line in injection molding is related to temperature control and distribution. Variable mold temperature techniques, also known as Variotherm mold technologies, were developed based on the principle that ideal molding conditions require a hot mold during the injection phase and a cold mold during the cooling phase [9]. Therefore, a temperature control system for both mold heating and cooling is needed: temperature measurements, heating, and cooling actuations.

Mold cooling is a well-established technique in conventional injection molding, while mold heating techniques have been introduced only recently. However, these process conditions have opposite effects on the cycle time: heating increases its duration, while cooling reduces it. Another important consideration is the effectiveness of heating, which is advantageous if the filling time is long, but becomes harmful in very fast filling. This is particularly true in micro-injection molding, where the injected mass is very small or in cases requiring high injection velocity.

Mold heating is essential to reduce specific molding defects, such as weld lines, and it also improves the surface quality of products and reduces molding pressure, residual stress, and clamping force. Several solutions were proposed to achieve these benefits, including circulation inside the mold of hot water, oil, or steam, or by using electric and electromagnetic induction heating, flame heating, and infrared heating [2,9].

However, all these solutions worsen process productivity and energy management. Indeed, the increase in the mold temperature also increases both the cycle time and the energy demand. Rapidly heating and cooling of massive parts is time-consuming and wastes energy, and this has significantly limited the application of the Variotherm concepts. To overcome these drawbacks, localized heating of mold portions during the injection was recently proposed [9], utilizing some thermal insulation layers embedded into the mold. However, these solutions significantly increase mold and process complexity, with negative effects on production costs.

1.2. – Mold cooling efficiency

Enhancing mold cooling effectiveness ensures rapid and uniform heat extraction from the molten polymer [1,2,9]. Thus, the mold design must consider this aspect by carefully evaluating geometry, material, and cooling channel layout.

Traditionally, in conventional steel molds, cooling channels are manufactured by drilling several straight holes within the mold core and around the cavity. This approach results in variable offset distances between the circular cooling channels and the complex-shaped mold cavity, leading to non-uniform heat extraction. Conformal cooling channels emerged as a superior solution to overcome this limitation and achieve more uniform cooling.

With their three-dimensional evolution and optimized cross-sections, these channels ensure uniform and effective heat removal across the cavity surface. Conformal cooling in bulk mold components is enabled by Additive Manufacturing (AM) [7,10–13] or by rapid tooling technologies [14,15]. When achieved with a hybrid additive/subtractive manufacturing approach, these solutions also become economically sustainable, combining conventionally pre-fabricated base workpieces, as a build platform, with additively generated functional features of minimized volume [16–18].

1.3. – Soft molds and additive manufacturing

While high-strength stainless steels are conventionally used to fabricate all mold components, the advent of AM has opened new scenarios [19–21]. Among these developments, several studies discuss soft mold inserts (or plates) with cavities made of polymers or composites via AM technologies, but maintaining a conventional steel mold base to guarantee the required mechanical stiffness and strength [20–23].

The main advantage of this approach is to shorten the product development and time to market by prototyping or producing a pre-series (below one hundred) of functional parts for testing and marketing purposes. For example, the feasibility and related limitations of polymer resins for injection mold fabrication were verified in [20]. Two photopolymer resins were used to fabricate 3D-printed mold inserts with cavities via stereolithography (SLA) to replace traditional steel molds. The thermal properties of resins and the cooling phase negatively affect some mechanical properties of the molded part (specifically reducing elongation at break) and extend the overall cycle time.

However, the resin thermal conductivity was not sufficient to achieve the requested part quality. Moreover, resin mold inserts are suitable for prototypes or small batches only due to mechanical limitations. Indeed, polymer or composite soft mold inserts exhibit cracking and chipping failure mechanisms due to their brittle behavior, thus limiting the number of molding cycles [20–22]. High strength and stiffness are often accompanied by high brittleness, which results in a low mold lifetime. Furthermore, concerning the thermal properties, the used materials have a heat deflection temperature (HDT) below 200 °C (ASTM D648–16), and they suffer erosion by melting of the cavity surface due to the high temperature of the injected polymer [20,21].

However, this approach does not improve the thermal regimes and the efficiency of the injection molding process, making the cooling phase sharply less efficient or completely inefficient, and therefore not implemented. In these cases, the cooling is obtained without circulating coolant in the mold, but by prolonging the cooling time, keeping the mold at temperatures below the material's glass transition temperature (T_g). This also results in higher cycle time, lower efficiency, and reduced productivity.

1.4. – Motivations, approach and novelty

Leveraging insights from these previous results, this study discusses a different research approach to overcome the limitations of prior mold design.

The main focus of this work is energy management and injection molding efficiency. These two objectives were pursued through a novel mold design, guided by three key drivers: KD1) Reduction of the thermally conductive mold core mass; KD2) Thermal insulation of the mold core; KD3) Mold weight reduction.

KD1 and KD2 guarantee faster thermal transients (KD1) and reduced heat dispersion (KD2), but these two key drivers are interdependent, as the reduced thermally-conductive mass is obtained with polymers, which also act as mold core thermal insulation. The KD3 is achieved with polymers for the mold large component (i.e., support plates), together with FEM-based and topology optimization of the components. KD3 reduced the mechanical energy required for mold motion during injection molding cycles and for handling during production turnover.

The novel mold concept was conceived with an apparently counterintuitive criterion: steel mold inserts with polymeric structural base mold components. The counterintuition is that polymers are apparently not suitable for mold structural components.

Finally, it is not negligible the contribution of this work to the Variotherm solution. In fact, in this case, more thermally reactive molds, characterized by faster thermal transients, are required to rapidly follow the thermal actuation required in Variotherm (e.g., high cavity temperature in injection and efficient cooling). The proposed concept significantly contributes to this targeted thermal behavior, enhancing Variotherm's performance, thereby improving quality and production rates in injection molding.

Therefore, a novel mold structure, composed of steel mold inserts (with cavities and cooling channels) and polymeric/composite base mold components, is proposed. These new hybrid molds do not offer the advantages of the conventional approach (i.e., rapid prototyping and small batches of products), but they also do not suffer from the associated drawbacks (i.e., thermal and mechanical weaknesses, poor part quality, inefficient cooling, extended cycle time). Indeed, they introduce new relevant advantages: mold thermally conductive mass, thermal insulation and lightweight design. This is an original approach since no previous works were found in the literature or known applications utilizing this structure.

Maintaining a steel mold core with the cavity made by AM technologies allows for achieving the advantages of conformal cooling and reduced cycle times. Indeed, polymeric/composite mold base components change the thermal behavior of the mold and the process, since they do not participate in thermal conduction and heat transfer. Beyond thermal benefits, using polymers and composites for mold components allows the design of lightweight molds with additional advantages in terms of mechanical energy savings during mold motion (opening/closing) and production turnover phases [23]. Finally, this new concept exploits all the advantages of additive manufacturing, such as full-digitalized design, increased mold geometry complexity and design freedom, thus enabling highly efficient conformal cooling. This comprehensive approach potentially represents a step towards a more sustainable injection molding process. Indeed, by both reducing the mold thermal conductive mass and introducing the thermal insulation for the mold core, this approach contributes to the development of a more efficient variotherm technique and conformal cooling system. Hereafter, conventional and innovative molds are compared in terms of materials, structure and energy consumption. The current technology baseline is depicted in Fig. 1.

In conventional molds (CM), all components are made of bulk steel. The heat also flows from the injected polymer to the mold (Fig. 1). A quote of heat is extracted from the mold ($\dot{q}_1$ *and* $\dot{q}_2$) by means of a water-cooling system (i.e., channels manufactured by drilling the bulk steel), see Fig. 1, b. An external chiller continuously cools down the water and controls its temperature, thus requiring additional electrical energy. Another quote of heat ($\dot{q}_3$ *and* $\dot{q}_4$) is wasted in the surrounding environment. The new approach is depicted in Fig. 2.

In unconventional hybrid molds (HM) design, the mold inserts are fabricated of steel, while the base mold components are made of thermal-insulating polymers or composites (Fig. 2, a). In this new concept, the heat ($\dot{q}_1$ *and* $\dot{q}_2$) is efficiently extracted from the mold inserts via conformal cooling channels, see Fig. 2, b. The heat does not flow in the surrounding environment because of the adiabatic interface between mold inserts and thermal-insulating base mold components, hindering conduction and convection heat transfer mechanisms. In this new concept, the extracted heat is moreover reused in other phases of the process, such as material drying or pre-heating, or heating injection machine subsystems. The residual heat is finally absorbed by the chiller.

It is worth remarking that the novelty of the hybrid mold is not just the combination of two different materials (steel and polymers), but a structured solution, where an optimized mold mechanical structure includes components made of different engineered materials, to enable enhanced thermal mold behavior (faster thermal transient, lower heat dispersion, lightweight mold). The enhanced mold behavior results in many advantages: 1) higher production rate (lower cycle times obtained with reduced cooling time); 2) Lower thermal energy waste by reducing the heat dispersion with the surrounded environment; 3) Faster molding startup; 4) lower heat extraction requirements for cooling; 5) lower mechanical energy for mold motion (opening/closing) within the molding cycle; 6) Lower mechanical energy committed for mold handling and change in production turnover.

This study aims to evaluate new multi-material hybrid molds using

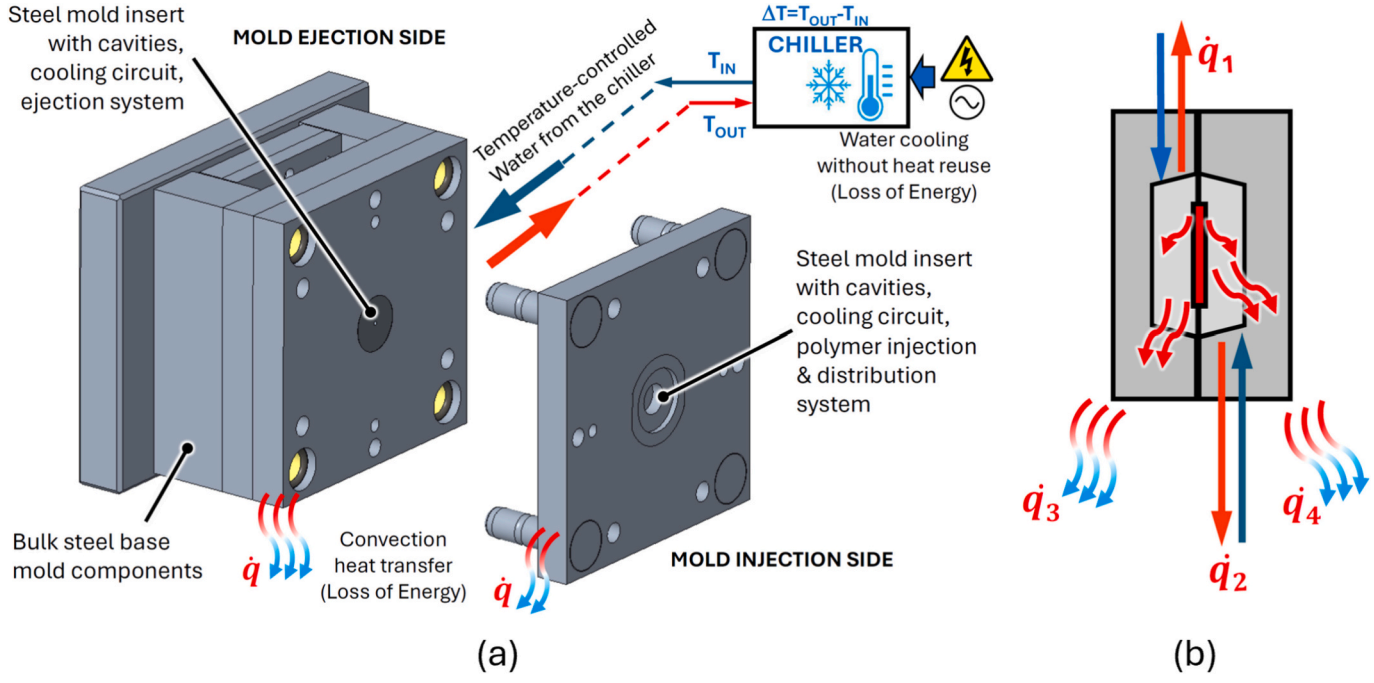


Fig. 1. Schematic of the Conventional mold (CM) design (a) and heat transmission scheme (b).

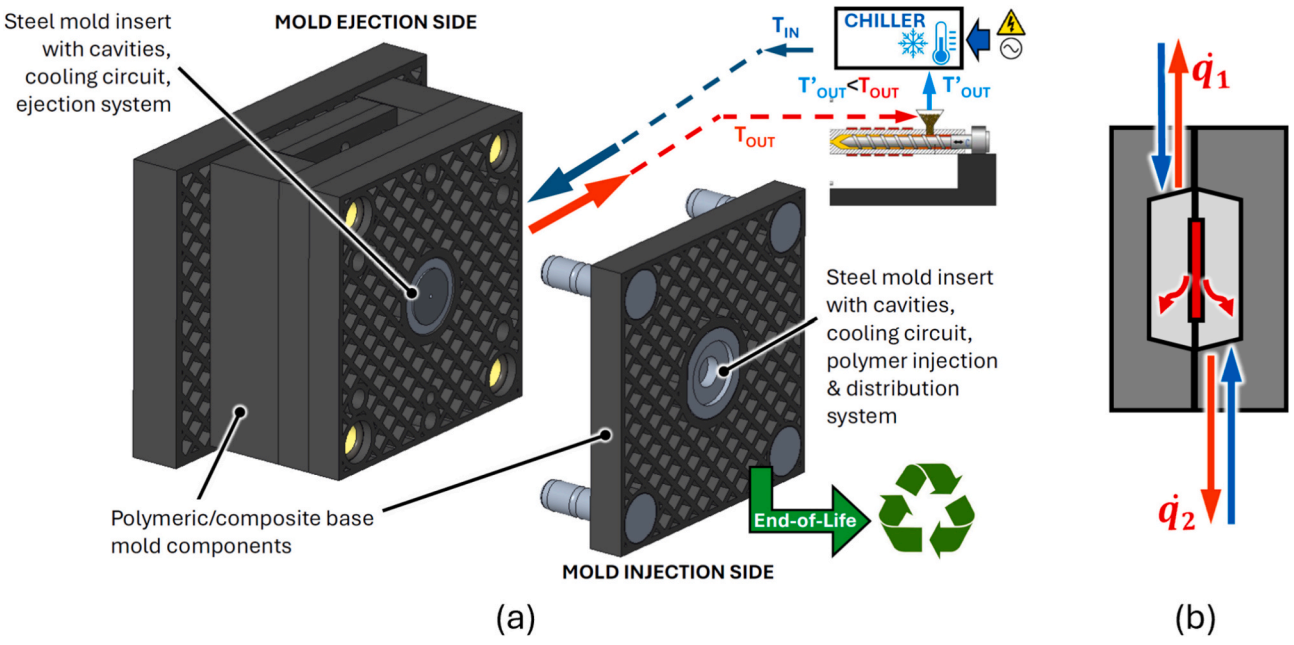


Fig. 2. Schematic of the unconventional hybrid mold (HM) design (a) and heat transmission scheme (b).

unconventional materials to optimize thermal energy management in the injection molding process. The experimental campaign was conducted to assess heat transfer dynamics, thermal transients' evolution, and overall energy benefits using both multi-material hybrid and conventional steel molds. Furthermore, the resulting experimental data were used to calibrate and validate a thermal numerical model. This model will be a powerful tool for mold performance assessment and design optimization, directly contributing to enhanced operating energy efficiency and sustainable manufacturing. Considering the approach depicted in Fig. 2, this work is focused on thermal transients and regimes in molding. It explores the advantages of thermal insulation of the mold core, comparing conventional and innovative molding processes, without the implementation of cooling. The paper is structured as follows: Section 2 presents materials, methods, and the experimental procedure, Section 3 is dedicated to the development of numerical modeling and simulations. Section 4 presents results and discussion, and Section 5 provides the conclusions of the work.

2. Mold design and fabrication

2.1. Mold design

In this work, the multi-cavity steel insert allows the production of two mini dog bone tensile samples with a thickness of 1 mm, length of 12 mm, and width of 1.5 mm in the narrow region and 3 mm in the larger one (Fig. 3) [24]. The total molded mass is about 78 mg, including sprue, cold runner channels, and cavities.

The mold inserts are assembled in two support plates on the injection (ISP) and ejection (ESP) sides. The conventional mold has bulky steel support plates, whereas the hybrid mold has mixed bulk-lattice polymeric support plates. The schematic of the two mold configurations is reported in Fig. 4).

Basically, in both molds – CM and HM – two main functions are requested of the support plates: 1) to keep the mold inserts in position; 2) to contribute to the mold guiding system, by assembling and coupling columns and bushes.

Support plates do not experience the high mechanical stresses that arise during the molding cycle (e.g., the clamping force exerted by the injection molding machine and the forces generated during the filling and holding phases). Indeed, the clamping force is transmitted from the ejection to the injection side through the steel mold inserts and the steel end plates behind the support plates. Mechanical stress arises in support plates due to forces transmitted by the couplings between columns and bushes during mold opening and closing. However, this stress is expected not to be critical, as both columns and bushes are assembled within the steel end plates.

These considerations are schematized in Fig. 5, where the mold's cross-sections show both clamping force transfer (a) and guiding

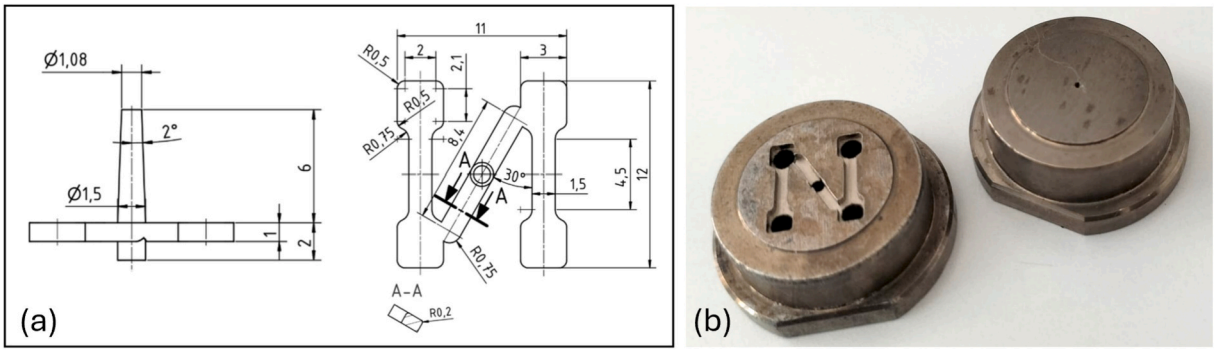


Fig. 3. Mold cavity design (a) [24] and steel mold inserts, ejection and injection side (b).

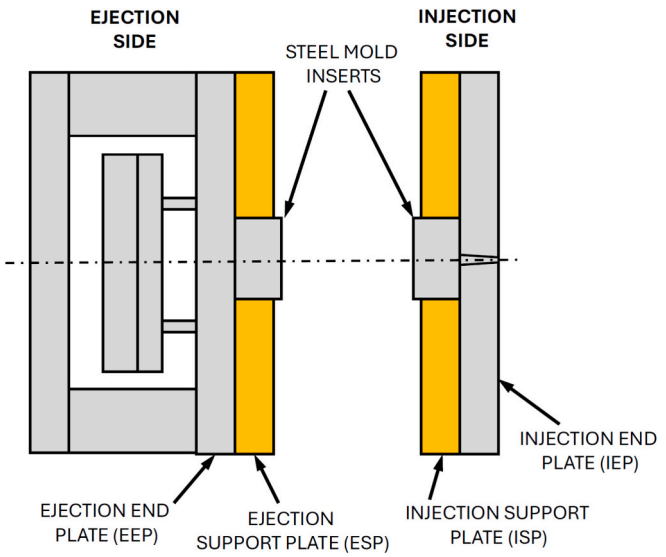


Fig. 4. Schematic section of two setups with different mold support plates (orange): CM with steel mold plates; HM with polymer mold plates. Both with steel mold inserts on both sides.

components reference positions (b). Note that there is no direct contact between the two support plates. A gap is present between them. On the contrary, mold inserts are compressed between the two end plates (EEP-IEP) by the clamping force. This detail guarantees the seal of the mold cavity along the parting surface on mold inserts. The design of the hybrid mold is presented in Fig. 6.

2.2. Hybrid mold materials

As reported in the introduction, the HM is characterized by support plates that are primarily demanded to thermally insulate the mold inserts, keep them at the correct positions, contribute to the mold guiding system, and allow the positioning of auxiliary sub-systems, such as thermocouples and mold cooling components.

Therefore, the feature requirements for these components are: i) low thermal conductivity; ii) stiffness, also at high temperatures; iii) high dimensional stability; iv) mechanical strength. These requirements are met by high-performance polymer and composite materials. Indeed, as is well known, in injection molding the mold is heated by the injected melt and kept at high temperatures in the range of 60–200 °C, depending on the injection-molded material, spanning from conventional polyolefins to high-performance polymers and composites, such as PolyEther-Ether Ketone (PEEK).

In the hybrid design, these temperatures are reached in steel mold inserts and locally in steel base mold components. However, the support plates should fulfill the requirements for maintaining dimensional stability and mechanical performance at high temperatures up to 200 °C. Only polymers/composites having high glass transition temperatures (T_g) and Heat Deflection Temperature (HDT) are excellent candidates for this application. Furthermore, high-dimensional accuracy and surface finishing are also important requirements for this application.

As reported in the literature, compared to other AM technologies, stereolithography (SLA) has superior dimensional accuracy and surface finish [20,21], and was therefore selected for the manufacturing of the HM support plates. Among SLA resins, only those specifically designed for high-temperature applications can be considered, specifically with high Tg and HDT. Table 1 reports a comparison of the mechanical properties of a conventional resin (White V05) and two high-temperature engineered resins (High Temp HT and Rigid10K).

Resins HT and Rigid10K were preferred over the standard White resin due to their higher HDTs. Despite Rigid10 K's higher stiffness and ultimate tensile strength, the HT resin has a higher HDT at 1.8 MPa, and therefore, it was selected for the HM manufacturing.

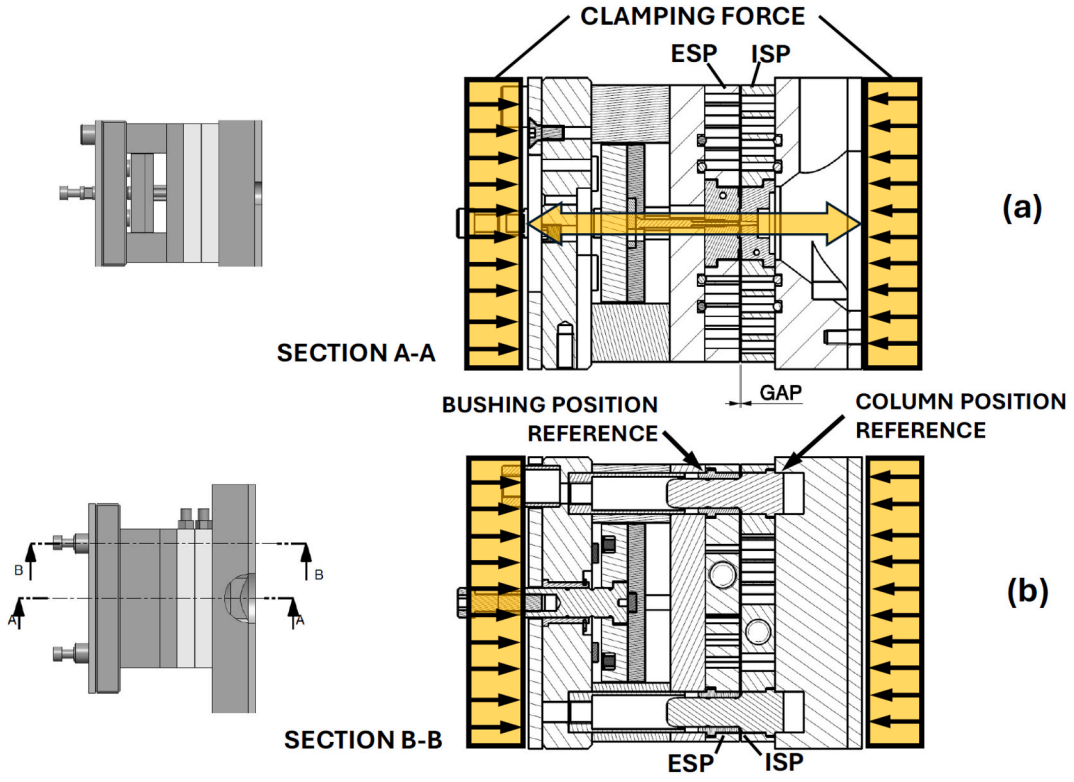


Fig. 5. Mold assembly drawing and cross sections. Section A with clamping force transfer inside the mold (a); section B with the reference positions of the guiding system components (columns and bushings) (b).

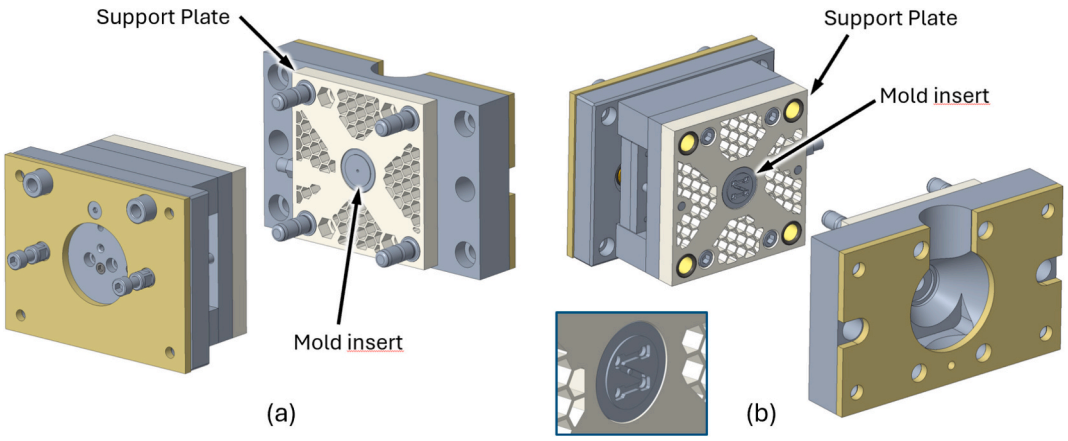


Fig. 6. HM design. CAD 3D views of the HM; injection side (a) and ejection side (b). Steel plates (grey), polymer plates (white), mold-press interface plates (yellow). (For interpretation of the references to colour in this figure legend, the reader is referred to the web version of this article.)

Table 1
Comparison of mechanical properties of photopolymer resins: White, High Temp, Rigid10K. (Source: Material datasheets, Formlabs Inc.)

Parameter	Units	White V5	High Temperature (HT)	Rigid 10 K
Ultimate tensile Strength (UTS)	MPa	61	49	88
Elongation at break (A %)	%	11	2.3	0.7
Tensile Modulus (E)	MPa	2650	2800	11,000
Flexural Strength	MPa	103	97	158
Flexural Modulus	MPa	2750	2800	9900
Notched Izod	J/m	29	17	20
Unnotched Izod	J/m	–	–	130
HDT @0.45 MPa	°C	62	238	238
HDT @1.8 MPa	°C	54	101	92
Thermal Expansion	$\mu m\ m^{-1}\ ^{\circ}C^{-1}$	–	75	41

2.3. Molds manufacturing

Each mold side (injection and ejection) consists of a mold plate and insert. Mold inserts were fabricated in X33CrS16 steel (Werkstoff 1.2085) with traditional cutting (milling and grinding) technologies. By maintaining the same steel inserts, Conventional steel Mold (CM) and Hybrid steel-resin Mold (HM) were tested. In CM, mold plates were realized as mold inserts (i.e., same material and manufacturing technologies). On the contrary, in HM, mold plates were fabricated of photopolymer resin Formlabs High Temp V02, engineered explicitly for high-temperature applications via Stereolithography (SLA).

The main mechanical properties of this material are suitable for the specific application [25] and are reported in Table 1 of Section S1 of the supplementary information. The polymer mold plates were designed with a bulk structure similar to bushes and columns for guiding and aligning the mold parts, and a hexagonal lattice structure in low-stress regions, as determined by topology optimization [26]. High-dimensional accuracy and surface finish are required for this application to ensure proper guiding and alignment of mold components. Therefore, some precautions in the manufacturing design, particularly in the SLA pre-processing step, are required, such as a geometrical compensation strategy and the implementation of an optimized process chain [27–29].

A Formlabs Form3 machine (Somerville, Massachusetts, USA) was used for the mold plates fabrication, by setting the following process parameters: layer thickness of 100 μm, part orientation flat on the build platform (XY plane) without base and supports.

Part post-processing consisted of three phases: 1) washing in high-purity (99%) isopropyl alcohol (IPA) for 20 min; 2) UV-curing in a Formlabs Cure machine for 120 min at 80 °C; 3) Annealing for 180 min at 160 °C in an oven Memmert UNE400.

Post-processing operations 2 and 3 improve the part's mechanical properties. Notably, annealing allows achieving a heat deflection temperature of 238 °C (HDT at 0.45 MPa, ASTM D648–16) [25], which is a relevant parameter for ensuring the required mechanical performance (stiffness and stability) at the required mold temperatures.

3. Experimental procedure

The experiments aimed to acquire thermal transients on the molds (conventional and innovative), such as mold temperature variations during the injection molding cycles, from the transient to the steady state regime.

The experimental tests were designed to demonstrate the hybrid mold's ability to fast warm-up (thermal transients faster than CM), store and retain thermal energy, thereby sharply reducing energy waste (i.e., through convection to the surrounding environment). These are two fundamental features of the HM.

To emphasize these aspects, the intensive water cooling was not implemented to avoid its disturbing effects, resulting in only minor evidence of the positive effects of thermal insulation and low thermal-conductive mass. However, the cooling was performed by keeping the molded part inside the mold cavity for 4 s, thereby transferring heat from the molded mass to the steel mold insert.

This latter solution is very common in micro-injection molding, as coolant or water circulation can cause a drop in mold temperature, which negatively affects the subsequent molding cycle. Therefore, at this stage of the study, the objective was primarily to isolate transient thermal effects rather than to emulate production scenarios.

Experimental molds were mounted on the micro-injection molding machine Formica Plast 1 K by DesmaTec, available in the CNR-STIIMA Lab. The machine's technical specifications include a maximum injected volume of 150 mm^3, a maximum injection pressure of 300 MPa, and a maximum injection rate of 3.5 cm^3/s.

Due to its suitability for high-performance mechanical parts manufacturing, the polymer Polyoxymethylene (POM, Ultraform N2320003, BASF Engineering Plastics) was selected for the injection molding. During the cooling phase, no coolant was used, aiming at bringing out the differences between the two molds.

Two different mold conditions were tested for injection molding cycles: C1) mold warm-up from ambient temperature using just the thermal exchange between the melt polymer and the mold during the cavity filling and employing CM and HM plates alternatively; C2) molds pre-heating by cartridge at 80 °C for CM plates.

In this way, the potential of hybrid solutions and the limitations of standard solutions in achieving the desired thermal conditions without an external heating source can also be highlighted. Indeed, in the context of the more sustainable injection molding process, reducing and recovering thermal energy without dispersing heat into the environment is paramount. Furthermore, experimental tests under different thermal conditions and mold materials allowed for the proper calibration of the numerical model, as discussed in the following sections. Detailed process parameters are reported in Table 2.

The machine was equipped with sensors to acquire the temperature data. The data acquisition (DAQ) system utilized four K-type thermocouples interfaced with as many Max6675 digital modules to convert the analog signal from the thermocouple to a 12-bit digital signal. The DAQ system architecture was based on Arduino Uno Hardware and a custom firmware routine. An additional Fluke 54 II thermometer was used to verify and calibrate the K-type thermocouples. The system allowed data acquisition from all four thermocouples with a resolution of 0.25 °C and a sampling period of 400 ms, corresponding to a frequency of $f_s = 2.5$ Hz. This frequency was optimal for monitoring the temperature variations during the molding cycles. In detail, the thermocouples were strategically positioned to provide a comprehensive overview of the temperature distribution within the mold. T1 and T4 were placed into specific holes within the movable and fixed inserts, respectively, close to the mold cavity (Fig. 7 a). Thermocouples T2 and T3 were located on the external surface of the mold, specifically on the top surface of the fixed (injection side) and movable (ejection side) mold plates, respectively (Fig. 7 b). Fig. 8 shows the injection molding machine and the experimental setup. Fig. 9 and Fig. 10 show the HM solution during mold opening and closing operations, and details of the experimental setup with all thermocouples positioned and connected to the acquisition system.

4. Numerical modeling

The acquired experimental data were used to calibrate the boundary conditions for the process simulations covering both CM and HM. As previously mentioned, the validation strategy was based on temperature measurements acquired from four thermocouples, with two sensors located within the mold inserts close to the cavities and two positioned on the external mold surfaces. This configuration allows capturing both the regions of highest heat flux and the external thermal response of the mold, providing a comprehensive assessment of the thermal behavior. Specifically, the hybrid mold (HM) configuration was used for calibration of the boundary conditions, while the conventional mold (CM) configurations were used exclusively for validation. Validation was performed under two different operating conditions (warm-up from ambient temperature and transient evolution after pre-heating at 80 °C). Except for the material properties of molds, the other process parameters and boundary conditions were the same for both CM and HM, mirroring the experimental setup.

Table 2
Process parameter settings.

Symbol	Description	Units	Value	
			CM	HM
T_m	Melt Temperature	°C	230	230
T_{mo}	Initial Mold Temperature	°C	20 or 80	20
V_{inj}	Injection speed	mm/s	150	150
t_f	Filling Time	s	0.4	0.4
t_h	Holding time	s	4	4
P_h	Holding Pressure	MPa	50	50
S	Piston stroke	mm	10	10
t_c	Average total cycle time (without coolant)	s	12	12
n	Number of injection runs	–	130 or 90	130

Numerical simulations were performed using Comsol Multiphysics v.6.1 (Comsol Inc., Stockholm, Sweden), a software that implements the Finite Element Method (FEM), often employed for analyzing complex multi-physics processes [30–33]. To reduce computational time, the 3D model of the mold block was simplified concerning the original one. In detail, the clamping plates were modeled as simplified domains combined with proper boundary conditions to consider the heat exchanges with the injector and the extractor systems. Fig. 11 displays an example of the complete setup model with polymeric support plates, while Fig. 12 shows the model as constructed in COMSOL Multiphysics.

After importing the modified 3D model into the software, all the boundary conditions were set as shown in Fig. 13, considering the injection process dynamics.

Since the model aimed to predict the thermal field during the process, the fluid dynamics of the injection were simplified while still explicitly modeling the polymer domain. In particular, the molten polymer was not described through fluid flow, but its thermal behavior during the filling phase was reproduced by means of a variable heat source, introduced to drastically reduce the computational time while capturing the dominant thermal phenomena.

This heat source increases the POM temperature within the cavity during the filling stage and is deactivated in the subsequent phases. It was carefully calibrated to ensure that the polymer temperature does not exceed the actual injection temperature.

Furthermore, the heat transfer coefficient of POM was defined as temperature-dependent to account for the different behavior in the molten and solid states. To incorporate, in a simplified manner, the effects of phase change, the heat transfer coefficient was increased in the temperature range corresponding to solidification (150–170 °C), thus accounting for the latent heat released during the transition.

This modeling strategy enables the simulation of multiple consecutive injection cycles within reasonable computational times, making it suitable for process and mold design support, while maintaining good agreement with experimental results.

Beyond heat exchange with the air, two key boundary conditions were calibrated: heat exchange with the injector and heat exchange with the extractors. These heat transfer coefficients were adjusted during the calibration phase on the HM configuration to reproduce the experimentally measured temperature evolution and should be interpreted as effective parameters accounting for complex contact and transient thermal conditions.

This approach allowed for an accurate numerical prediction with reduced computational time, avoiding the high complexity of modeling the entire press. More specifically, the heat transfer coefficient (HTC) was set high (260 W/m^2K) at the injection location during the filling and holding phases to account for the direct contact and pressure applied to the sprue. This value was then reduced in subsequent phases to account for the partial detachment of the injector and the presence of an air gap (130 W/m^2K).

At the ejector locations, the HTC linearly decreased from 500 to 100 W/m^2K. This accounts for greater heat removal during the initial cycles, when the ejector system is colder, and a progressively reduced cooling effect as the ejection system warms up and approaches thermal equilibrium.

For transient simulations of the warm-up without pre-heating, the system's initial temperature was set to ambient temperature, while in the CM case, it was pre-heated to 80 °C. The initial conditions were selected based on the thermocouple data acquired at the start of the first cycle. All critical process time parameters, such as holding time, filling time, and cooling time (without coolant), were managed using Comsol's events interface module to accurately replicate the experimental process evolution.

The three-dimensional mesh consists of 406.670 tetrahedral elements, with a maximum size of 1 mm for cavities and inserts, and 5 mm for other components. These parameters represent a good trade-off between an accurate geometric representation and a reasonable

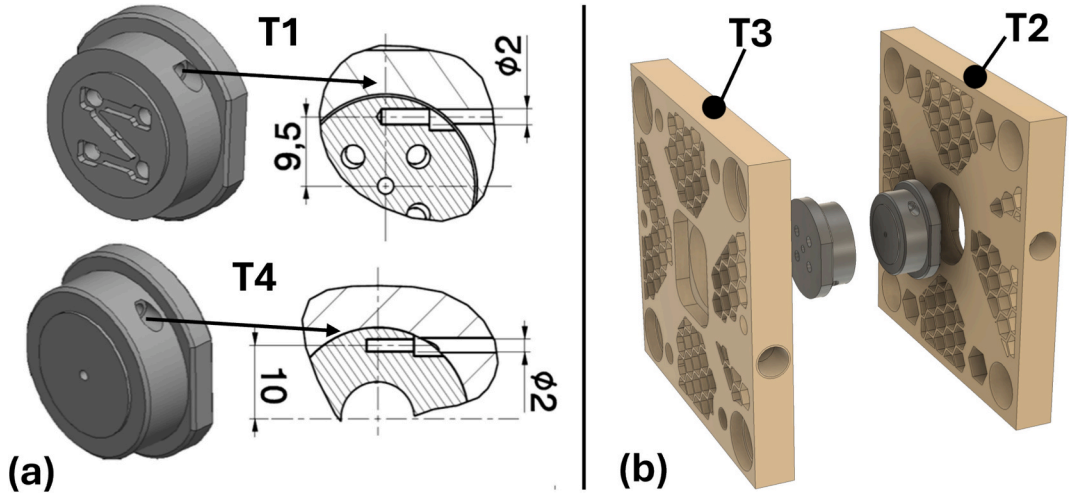


Fig. 7. Thermocouples placement: (a) insert, (b) plates.



Fig. 8. DesmaTec Formica 1 K machine plus the integrated sensorization setup.



Fig. 9. Hybrid steel - resin mold solution during closing and opening operations.

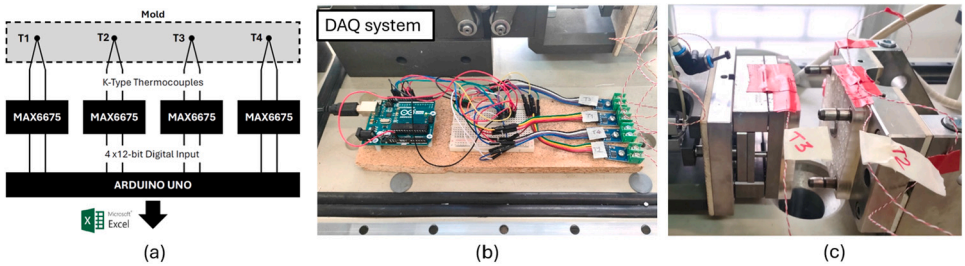


Fig. 10. Experimental setup of the HM. Block diagram of the DAQ system (a); DAQ system hardware and electrical connections (b); Thermocouples placement on the mold (c).

computational efficiency. Based on the experimental tests, 130 and 90 cycles were simulated for the warm-up without pre-heating and with pre-heating, respectively. The used process parameters are detailed in Table 3, while Table 4 provides the material properties sourced from material datasheets. The numerical simulations took an average time of 6 min for each injection molding cycle using a 13th Gen Intel® Core™

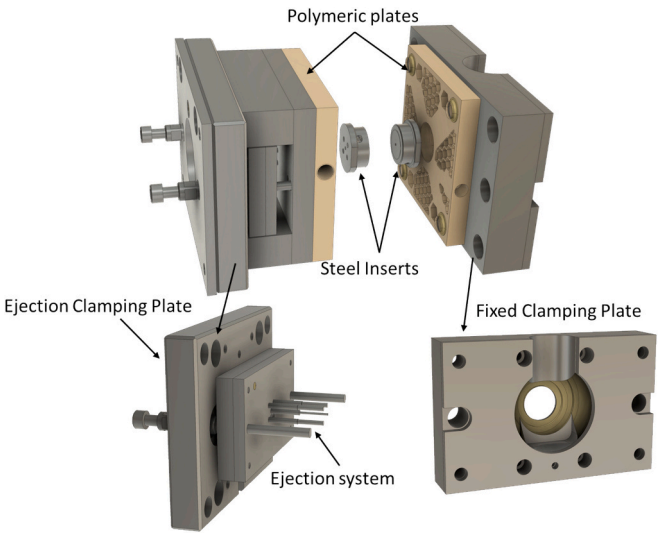


Fig. 11. 3D model of the mold block with polymeric plates.

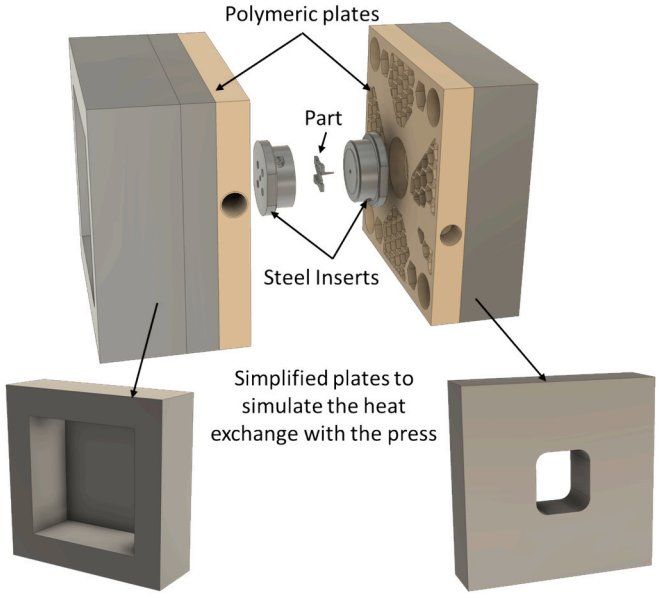


Fig. 12. Model (polymer plates) used in COMSOL Multiphysics with simplified clamping plates.

i7–13,700 (2.10 GHz), RAM 32 Gb, and graphics board Nvidia T1000 equipped with 8 Gb memory.

5. Results and discussion

5.1. Comparison between numerical and experimental data

Data acquired during the experimental campaign were compared with results from numerical simulations. As mentioned before, the boundary conditions were calibrated using the experimental outputs from the HM test, while the two CM conditions were used as a validation dataset. Fig. 14 and Fig. 15 show the experimental-numerical comparison of temperature evolution at the thermocouple locations for the complete campaign with the HM system. To provide a clearer analysis, Fig. 14 explicitly shows the temperature evolution within the inserts (T1 and T4), while Fig. 15 presents the evolution on the external mold surfaces (T2 and T3). The analysis of the graphs shows that temperatures are continuously increasing and, apparently, never reach a steady state. Under these conditions, the process appears to be out of control, but this is due to the intentional deactivation of the cooling system. Of course, it is expected that the CM steel mold will bring the process to a thermal equilibrium point where the injected heat $\dot{q}_m$ by molded part is counterbalanced by the heat $\dot{q}_t$ transmitted by convection to the ambient air and by conduction to surrounding press components. Therefore, CM will find a steady state thermal working point where $\dot{q}_m = \dot{q}_t$. On the contrary, HM has adiabatic interfaces due to the polymeric support plates, which hinder heat transmission, resulting in a dangerous temperature increase above the optimal ejection temperature.

The Fig. 14 reveals three distinct thermal regions for the mold insert temperature on the ejection side (T1, green graph): R1) warm-up region, from time $t_0 = 0$ s up to $t_1 = 100$ s (approximately the first 10 cycles); R2) mid-region, from time t_1 up to $t_2 = 700$ s; R3) Quasi-steady state region, for time higher than t_2, [700–1600]s. The numerical model demonstrates good predictive capabilities of temperature in the R1 region, with a rising transient almost superimposed on the experimental one. In the mid-region R2, the prediction fidelity gets worse, showing experimental values higher than numerical ones. This deviation is also kept in the third region R3, without a significant variation. A similar trend is shown by the mold insert temperature on the injection side (T4, blue graph). In the third region R3, the numerical prediction of T4 is affected by a reduced deviation compared to T1.

It is worth noting that the temperature spike and subsequent stabilizing transient observed in the HM data (Fig. 14) around $t = 300$ s was due to a part ejection failure, which required a manual removal of the part from the mold cavity by the operator. This specific perturbation was not included in the numerical model. It took about 400 s (from 300 to 700 s) to restore the effects of the perturbation (or disturbance) introduced by the machine stop of about 25 s required to remove the trapped part from the cavity.

The graphs clearly show that the calibration of the boundary conditions was effective, since the temperature evolution within the inserts was accurately captured throughout the cycles. At the quasi-steady state regime, the deviation for T4 was only −2 °C (72 °C actual vs 70 °C predicted) and − 4 °C in T1 (50 °C actual vs 46 °C predicted).

In the early cycles, on the external mold surfaces, experimental temperatures rose faster than numerical prediction, with a maximum deviation of −5 °C. However, during the final cycles, these deviations narrowed significantly to −2 °C for T2 (35 °C actual vs 33 °C predicted) and − 3.5 °C for T3 (30 °C actual vs 26.5 °C predicted). These small deviations suggest that the actual material's thermal conductivity might be higher initially but decreases as the temperature rises. In contrast, the simulation used a constant thermal conductivity value, which provided a better match after multiple cycles despite the initial underestimation.

To conclude the analysis of data for the HM, the numerical model is capable of an overall good prediction with deviations on temperature below 5 °C. Its performance is best on steel mold inserts in the warm-up region R1, but worse in the mid-region R2 at the end of the warming transient. Finally, in the quasi-steady state region R3, the predicted temperature deviation does not change in the interval. This demonstrates that the model has an integrative behavior (i.e., prediction error almost equal to the sum of errors in the previous regions), but invariant in the quasi-steady state region. A complete analysis of the prediction error of the numerical model in the case of the HM system is reported in Section S2.2 of the supplementary information.

Fig. 16 and Fig. 17 present the experimental-numerical comparison for the CM system starting from 20 °C. As expected, since the thermal conductive mass of HM is lower than CM, a higher sensitivity is observed in temperature measurements of HM, with higher values of standard deviation.

As previously mentioned, only the material properties of mold plates were changed in the model; the boundary conditions remained identical to those used in the HM system simulation. Also in this case, the numerical prediction within the inserts was very accurate, showing an almost constant deviation of about −2 °C for both T1 and T4.

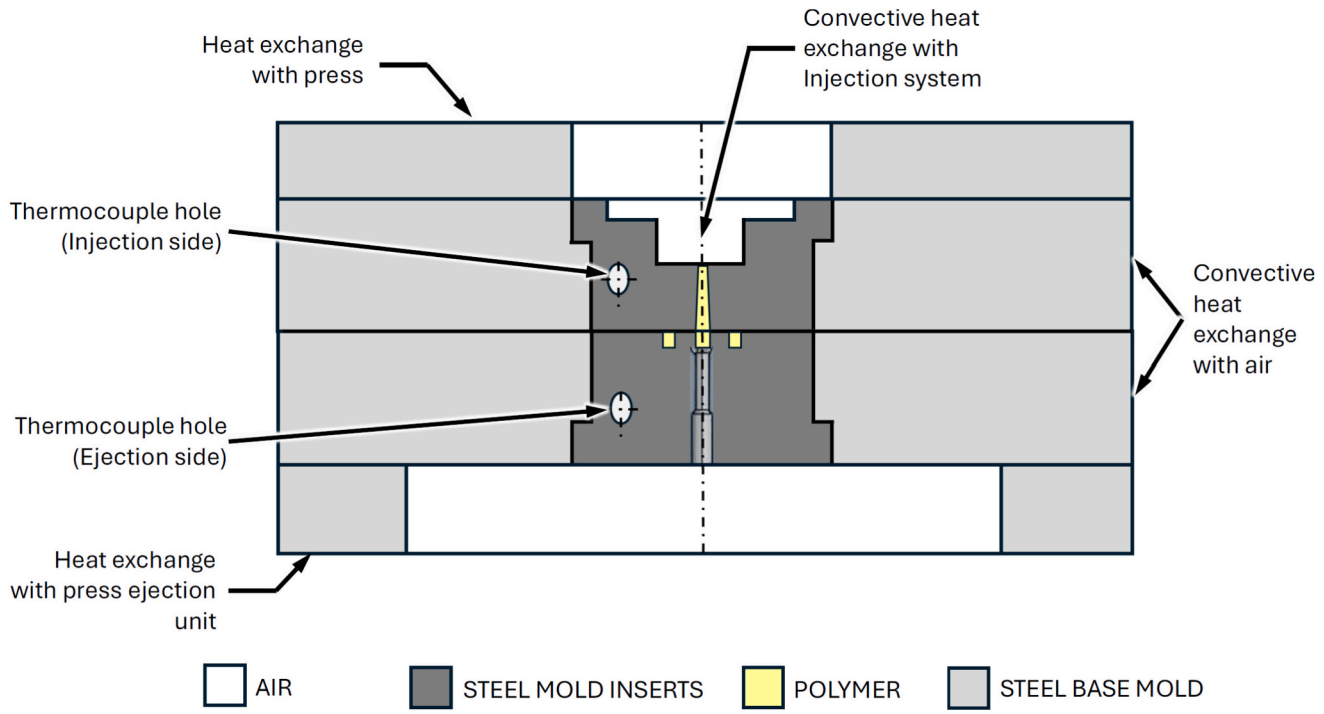


Fig. 13. Boundaries set in Comsol Multiphysics.

Table 3
Process parameters and boundary conditions set within the numerical model.

Process parameter	Units	Value
Melt temperature	°C	230
Filling time	s	0.4
Holding time	s	4
Cooling time (without coolant)	s	4
Mold open/close time	s	3.6
Initial insert temperature	°C	20 (HM), 20 and 80 (CM)
Initial support plate temperature	°C	20 (HM), 20 and 65 (CM)
Initial clamping plate temperature	°C	20 (HM), 20 and 60 (CM)
Air (ambient) temperature	°C	18
Injector temperature	°C	230
Ejection temperature	°C	for CM 18 or 80, for HM 18
HTC with air	$W/(m^2K)$	30
HTC with injector	$W/(m^2K)$	260 (filling+holding), 130 (cooling)
HTC with ejectors	$W/(m^2K)$	Linear decrease (500 → 100) in 500 s

Table 4
Material properties implemented within the numerical model.

Material property	Symbol	Units	POM	X33CrS16 Stainless steel	High-Temp resin V02
Density	ρ	g/cm^3	1.4	7.8	1.3
Thermal conductivity	K	W/(mK)	0.14	20	0.31
Heat capacity at constant pressure	c_p	J/(kgK)	f(T), 2137 @ 230 °C 16000 @ 150 °C	500	2700

Similar observations regarding thermal conductivity can be made on the external mold surfaces in the CM system. For T2, the initial deviation of −4 °C was reduced to −2 °C (36 °C actual vs 34 °C predicted) by the last cycle. Conversely, for T3, an almost perfect match was found during the initial cycles, but an overestimation of +3 °C (30 °C actual vs 33 °C predicted) in the last cycle. This behavior could be attributed to the cooling of the movable plate during the mold opening/closing stages, a phenomenon not fully simulated in the numerical model. A first-order approximation of this effect could be introduced by increasing the air heat transfer coefficient on the movable side during the opening phase; however, its influence is expected to be limited compared to the dominant heat transfer mechanisms governing the process, and it is less pronounced in the polymer plate due to its insulating properties.

The analysis of the prediction error of the numerical model in the case of the CM system is reported in Section S2.3 of the supplementary information.

Comparing the performances of HM and CM systems, the graphs of temperatures consistently show that the injection side is typically warmer than the ejection side in both setups. A key difference lies in the mold core's thermal transient, which was significantly faster in the innovative hybrid solution than in the conventional steel mold. This can be attributed to the HM's lower conductive mass and thermal insulation of the surrounding polymeric/composite support plates. Comparing the internal temperatures, HM consistently presented higher values, with an average difference of about 30 °C concerning CM (72 °C vs 46 °C) on the injection side. The temperature difference between the injection and ejection sides was approximately 20 °C in the HM system, while it was only about 5 °C in the conventional mold. This highlights HM's role as an insulating support for the steel insert, resulting in higher core temperatures and increased thermal sensitivity, but lower thermal energy dispersion.

The HM's internal components' thermal transient was characterized by a rapid exponential rise followed by a quasi-linear trend. In contrast, the CM system showed a minimal exponential rise, with the linear trend being predominant. Interestingly, the slopes of these linear trends were nearly identical (around 2–3 °C/200 s). Therefore, in continuous long-term molding, the regime temperatures tend to stabilize at higher temperatures in HM due to its low thermal inertia. This also demonstrates the potential to store and better manage thermal energy with polymer plates.

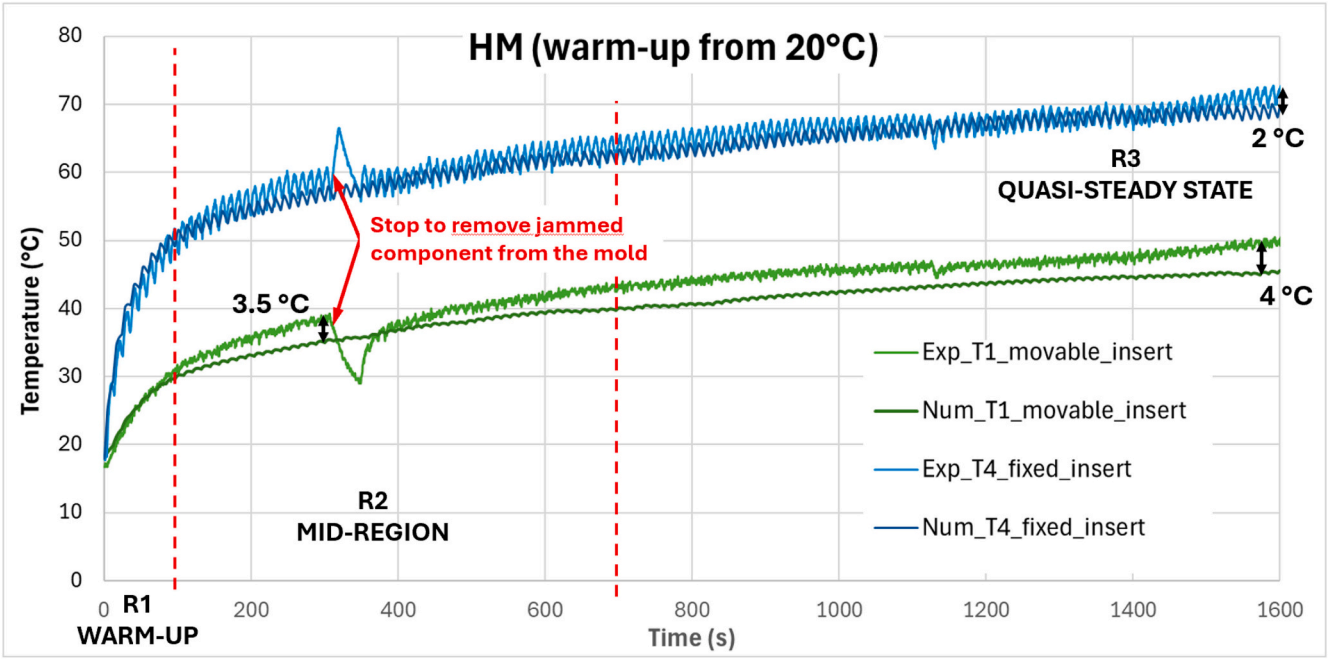


Fig. 14. Experimental-numerical comparison of temperature transients acquired by the thermocouples located within the mold inserts (HM system).

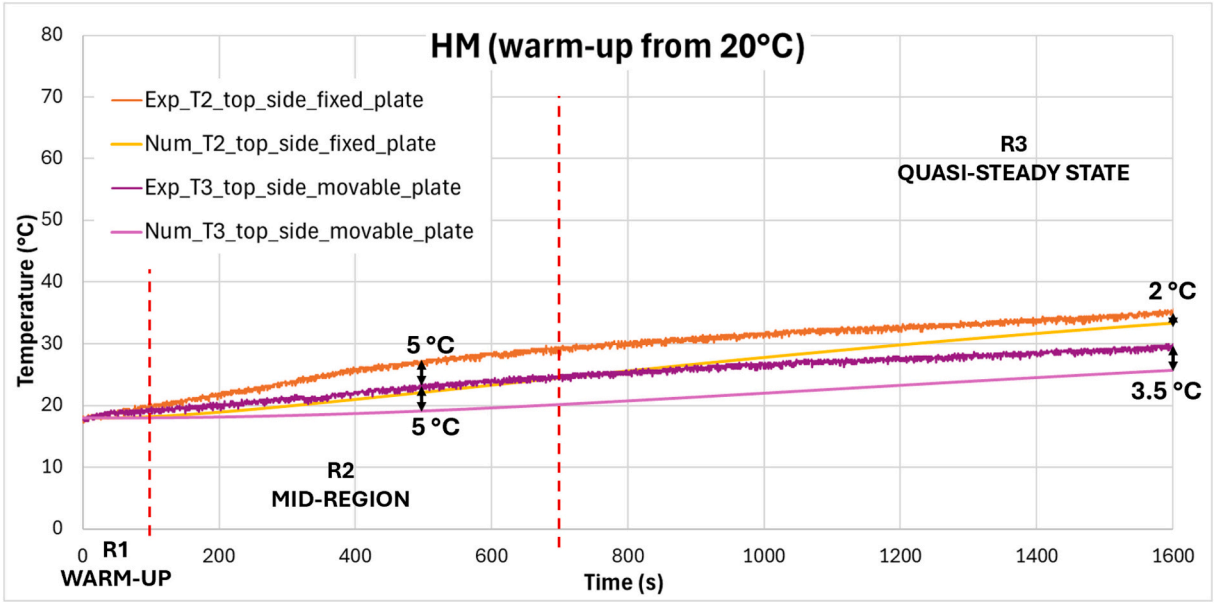


Fig. 15. Experimental-numerical comparison of temperature transients acquired by the thermocouples placed on the mold external surfaces (HM system).

From this point of view, Fig. 18 visually confirms the findings by comparing the simulated thermal fields at the end of the last cycle. The numerical prediction validated the experimental evidence, clearly showing lower thermal energy dispersion in the HM system. Indeed, in the HM system, thermal energy was concentrated primarily within the inserts, whereas in the CM system, it was dispersed throughout the entire block mold.

The final test concerned the evaluation of temperature evolution in the CM system pre-heated at 80 °C. Fig. 19 and Fig. 20 display the experimental-numerical comparison similarly to the previous analyses. Also, in this case, the results again confirmed the accuracy of the numerical prediction. Specifically, for T4, the numerical prediction was very close to the measurement. In contrast, in T1, a faster cooling in the simulation compared to experimental data was observed, resulting in an underestimation of 4 °C during the last cycle (58 °C actual vs 54 °C predicted). This numerical discrepancy can be attributed to the differences between the actual thermal field after initial pre-heating and the initial conditions set in the simulation. Indeed, as expected, the cartridge heating in the experiment caused a variable temperature distribution within the mold block. In contrast, the simulation initialized the inserts and the plates with a uniform temperature based on the thermocouples' measurements at the start of the first cycle. This aspect had less influence on the temperature evolution on the mold's external surfaces, where the maximum numerical discrepancy was only 1.5 °C.

The observed outputs evidenced the challenges for the CM system in maintaining an isothermal process without an external heating source. Despite the lack of dedicated cooling channels, the system's temperature tended to stabilize at least 15 °C lower than the initial one within the

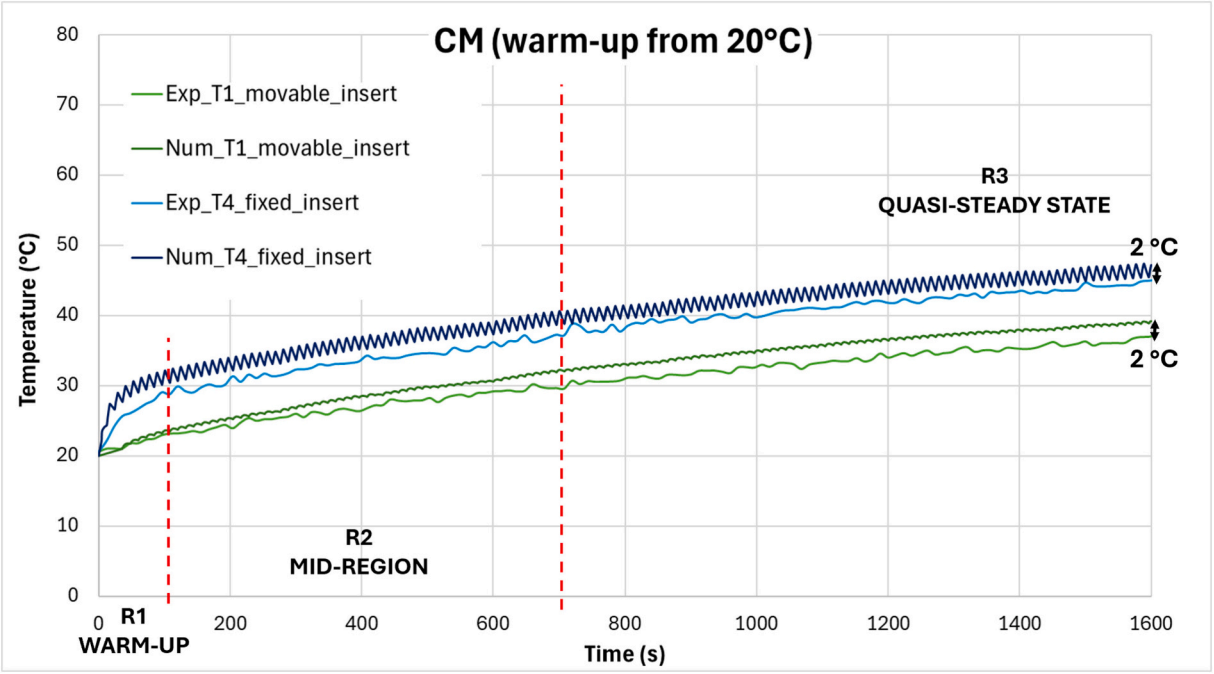


Fig. 16. Experimental-numerical comparison of temperature transients acquired by the thermocouples located within the mold inserts (CM system).

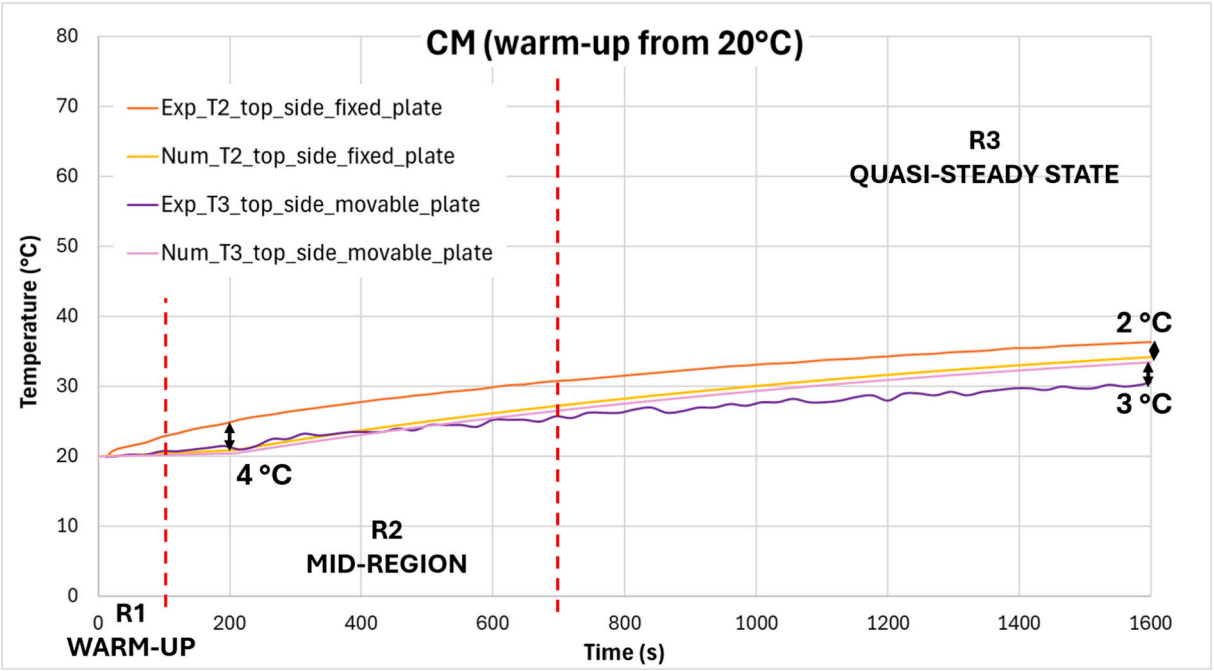


Fig. 17. Experimental-numerical comparison of temperature transients acquired by the thermocouples on the mold external surfaces (CM system).

cavities. Maintaining constant and controlled temperatures ensures that final components possess uniform properties and characteristics.

5.2. Dimensional characterization of injection molded samples

Due to the small scale of the samples, even minor deviations in geometry or weight can impact product quality, functionality, and performance. Therefore, dimensional measurements were carried out using a Mitutoyo digital caliper (resolution 0.01 mm) on ten specimens randomly extracted from each of the three batches (mold warm-up for CM and HM plates and mold pre-heating for CM plates). The selected dimensions for dimensional control were the dog-bone length, the width at the mid-section, and the thickness. These assessments drive process optimization and allow for a thorough evaluation of process stability. This is crucial for ensuring the accuracy of data used in the simulation model setup and validation.

Table 5 reports the average values with their corresponding standard deviations, indicating the overall successful replication, evidenced by low standard deviation values. As clearly shown in Fig. 21, for the conventional system (CM), dimensional deviations from nominal mold values are generally close to the nominal POM shrinkage (2.1%, ISO 2577294-4). This suggests good dimensional accuracy for parts obtained

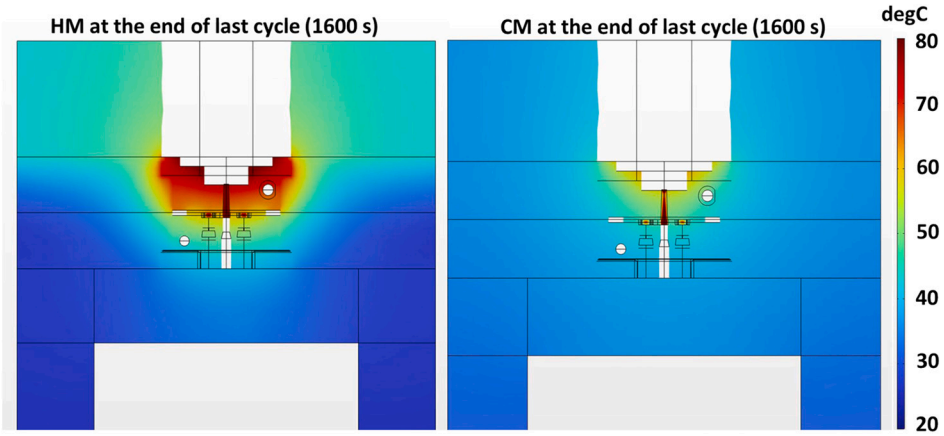


Fig. 18. Comparison of simulated thermal fields at the end of the last cycle: the HM system shows temperatures within the insert higher than 30 °C than the CM system.

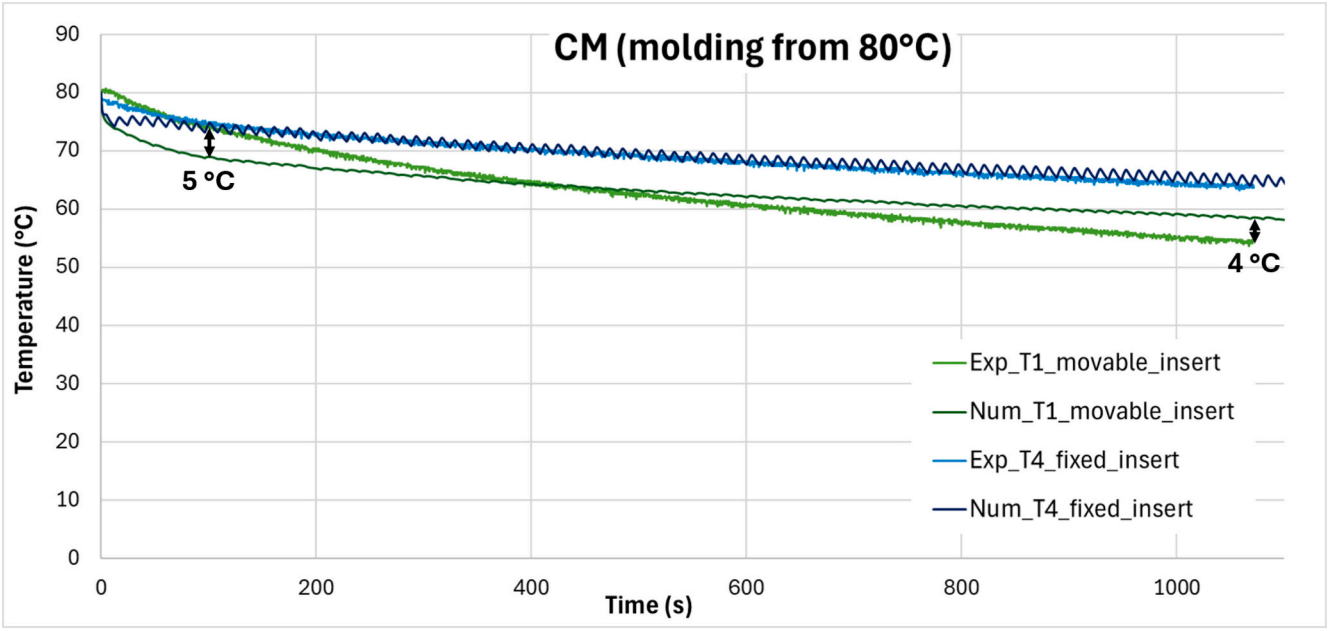


Fig. 19. Experimental-numerical comparison of temperature transients acquired by the thermocouples within the mold inserts (CM system pre-heated to 80 °C).

with the CM system. Conversely, parts produced by the hybrid system (HM) without cooling exhibit higher deviations across all measured parameters, between −2.5 and − 6.7%.

C.I.: 95% Confidence Interval calculated using the Student's T-distribution.

As previously stated, the injection molding parameters were selected based on previous experience and tests. They were not optimized, particularly for part accuracy and shrinkage control. In this section, the aim is to characterize the molded part to demonstrate the feasibility of the innovative process.

The main result is that the samples molded with the HM are affected by a higher volumetric shrinkage (Fig. 21, Table 5). These results can be justified by considering the thermo-mechanical properties of the POM material and the specific differences between the two molds. As shown in Figs. 14 and 16, the temperatures of the HM mold inserts are always higher than those of the CM mold inserts. To evaluate the effects of these temperatures on the specimens' dimensions, the molding cycle should be evaluated on the pvT diagram of the material. Fig. 22 shows the pvT diagram of the POM BASF Ultraform® N2320 [34]. The first step of this analysis is the identification of the pvT transformation curve. Table 2 reports the holding pressure of 50 MPa, which is assumed as the cavity pressure during the holding and cooling phases. On the pvT diagram, the closest curve is for $p = 40$ MPa. At a specific time, such as $t = 1200$ s, Figs. 14 and 16 give the mold insert temperatures of $T_{HM}(1200s) = 68$ °C and $T_{CM}(1200s) = 45$ °C, for HM and CM molds, respectively. With a graphical procedure, it is possible to derive the corresponding specific volumes at the ejection of the part, as depicted in Fig. 22. The same data can be derived from the pvT table (Supplementary Information, Section S3, Table 3). The calculated values for CM and HM, respectively, are:

- v_{eCM} (45 °C, $p = 0$ MPa) = $0.7181 \cdot 10^{-3}$ m^3/kg
- v_{eHM} (68 °C, $p = 0$ MPa) = $0.7285 \cdot 10^{-3}$ m^3/kg.

The volumetric shrinkage in the molded part is proportional to the difference between the specific volume during part ejection (v_{eCM}, v_{eHM}) and that at ambient temperature (i.e., $T = 20$ °C, $p = 0$ MPa), which in this case is equal to $v_{20,0} = 0.7069 \cdot 10^{-3}$ m^3/kg (Supplementary Information, Section S3, Table 3). Therefore, greater shrinkage occurs as the ejecting temperature increases [35]. In the results, the specific volume differences are:

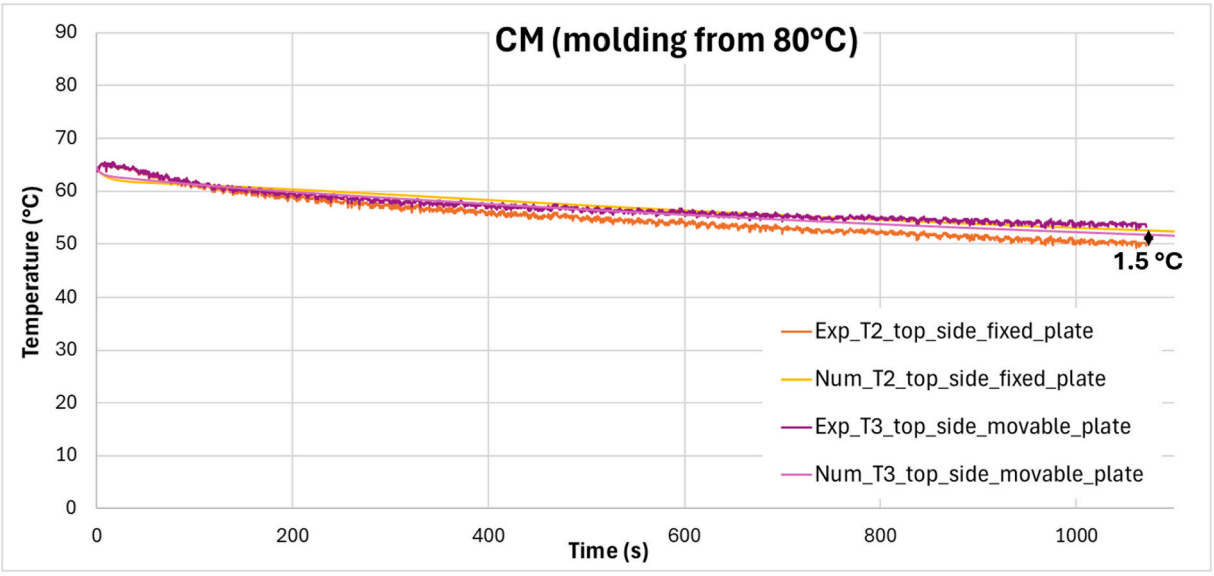


Fig. 20. Experimental-numerical comparison of temperature transients acquired by the thermocouples on the mold external surfaces (CM system pre-heated to 80 °C).

Table 5
Sample dimensional characterization.

Dimension (nominal)		Units	Experiment		
			CM warm-up	CM pre-heating	HM warm-up
Width (1.5 mm)	Measure[1]	mm	1.47 ± 0.04	1.46 ± 0.01	1.40 ± 0.02
	Dev. %[2]	%	−2.0	−2.7	−6.7
	CI[3]	mm	1.44–1.51	1.45–1.48	1.39–1.41
Thickness (1.0 mm)	Measure[1]	mm	0.98 ± 0.02	0.97 ± 0.01	0.96 ± 0.01
	Dev. %[2]	%	−2.0	−3.0	−4.0
	CI[3]	mm	0.97–1.00	0.96–0.98	0.95–0.96
Length (12.0 mm)	Measure[1]	mm	11.8 ± 0.05	11.8 ± 0.02	11.7 ± 0.03
	Dev. %[2]	%	−1.7	−1.7	−2.5
	CI[3]	mm	11.75–11.84	11.74–11.78	11.72–11.76

[1] Mean ± standard deviation.
[2] Dev. is the deviation of the mean from the nominal value.
[3] CI is the 95% Confidence Interval calculated using the Student's T-distribution.

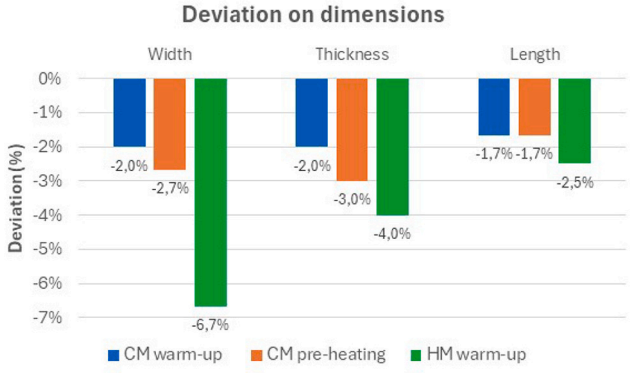


Fig. 21. Deviations of measured specimens from nominal mold dimensions.

$$\Delta v_{CM} = v_{eCM} - v_{20,0} = (0.7181 - 0.7069) \bullet 10^{-3}\frac{m^3}{kg} = 0.0112 \bullet 10^{-3}\frac{m^3}{kg} \quad (1)$$

$$\Delta v_{HM} = v_{eHM} - v_{20,0} = (0.7285 - 0.7069) \bullet 10^{-3}\frac{m^3}{kg} = 0.0216 \bullet 10^{-3}\frac{m^3}{kg} \quad (2)$$

The Δv_{HM} is higher (+92%) than Δv_{CM}; therefore, the samples molded with the HM are affected by a higher volumetric shrinkage, and this justifies the results reported in Table 5 and Fig. 21. The parts ejected at a higher temperature from the HM continue to shrink outside the mold, and the overall shrinkage is higher than those ejected at lower temperatures from the CM. Conversely, the CM cavity "freezes" the molded part geometry when ejected at lower temperatures. These results were expected since it is well known that the ejection of molded parts at high mold temperatures results in higher shrinkage [35]. However, this is not an issue since shrinkage and dimensional accuracy can be controlled by optimizing the process parameters (i.e., higher holding pressure), or by activating efficient cooling and mold temperature control. The material pvT diagram and the table of specific volume values are reported in Section S3 of the supplementary information.

However, the characterization demonstrates the consistency of results across the different thermal regimes, explaining the deviations in molded-part dimensions.

Beyond the presented experimental tests, the HM had a life of about 500 cycles, and failure occurred on polymeric support plates due to a cracking mechanism. In detail, the cracks originated from the cylindrical seats of the bushes and the columns of the mold motion-guiding system, thereby confirming the hypothesis regarding mechanical stress on the support plates stated in Section 2.1.

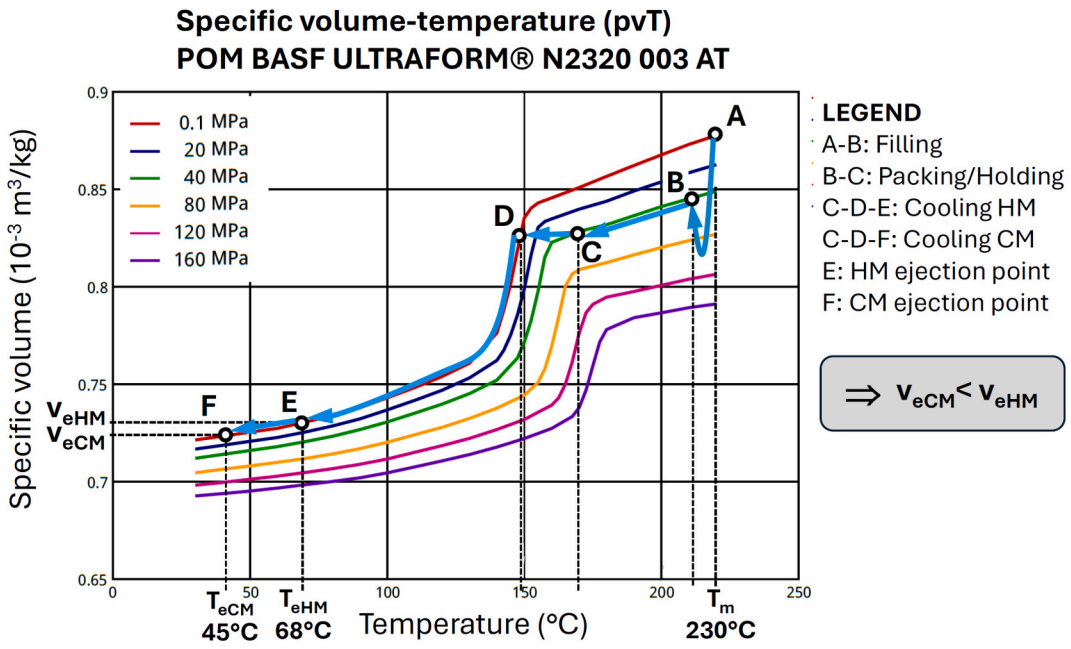


Fig. 22. pvT diagram of POM [34]. The molding cycle is described by the clear blue arrows. All phases are identified by the legend. The estimations of specific volumes v_{eCM} and v_{eHM} for CM and HM molds, respectively, are derived at the ejection temperatures that occurred at time 1200s of the experimental tests.

5.3. – Comparison of the energy commitment within the molding cycle

The numerical simulation enabled the estimation of the energy stored by the insert to evaluate the energy consumption of the two different configurations. The stored thermal energy was calculated from the simulated temperature field by integrating the sensible heat over the insert volume, according to the following relation:

$$E = \int_V \rho \; c_p \; (T - T_{ref}) \; dV \tag{3}$$

where ρ is the material density, c_p is the specific heat capacity, T is the local temperature, and T_{ref} is a reference temperature. For the evaluation of the energy stored per cycle under quasi-steady-state conditions, T_{ref} was defined as the temperature at the beginning of each cycle. Conversely, for the estimation of the total accumulated energy during the warm-up phase, T_{ref} was defined as the initial temperature at time $t = 0$ for each node of the insert mesh. Data are summarized in Table 6.

Considering the last cycle before the machine shut down, when a quasi-stationary regime is reached, the energy stored by the inserts at each cycle is estimated to be 3.06 J and 3.18 J (+3.92%) for the CM and HM systems, respectively.

Operating at full capacity, the insert stops accumulating heat significantly in both solutions. Considering the heating up phase, the warm-up from the ambient temperature until the first machine stop occurred at cycle $N = 133$, the overall thermal energy stored by the inserts is 1048.0 J and 1622.6 J for the CM and HM, respectively. With the same energy injected into the system, compared to the HM configuration, the CM process shows an energy loss of −547.6 J (−54.83%). Although energy assessments are preliminary estimations of actual consumption in the process, the thermal insulating capacity of the polymer can improve the energy efficiency of the mold.

In addition, even if the energy-related quantities are derived from the simulated temperature field, the accurate prediction of temperature evolution also supports the reliability of the energy analysis.

The energy stored within the inserts can be extracted using high-efficiency systems and reused for other phases of the molding process. The higher the stored energy, the greater the harvested quantity of energy, since the waste of energy in the surrounding environment is reduced.

Table 6
Comparison of numerical estimation of energy stored in the insert in CM and HM systems.

Parameter	Units	CM	HM	ΔE_{HC}	ΔE_{HC}%
Energy stored in the mold insert @Steady State	J/ cycle	3.06	3.18	+0.12	+3.92%
Total energy stored in the mold insert on N = 133 cycles	J	1048.0	1622.6	+574.6	+54.83%

5.4. – Mold weight reduction

One of the target benefits of the novel mold is the reduced weight. The weights of support plates (CM and HM) were measured using a digital balance (MAUL studio, Switzerland, Max 2.5 kg, resolution 2 g). Measurements are reported in Table 7.

The average mold weight reduction is −88.2%, a remarkable result achieved not only by substituting heavy steel with a lightweight polymer, but also through mechanical structural FEM analysis and topology optimization of the support plates [26].

5.5. Preliminary data for sustainability assessment

The sustainability assessment of this work was partially addressed in recent publications by the same authors [26,36,37].

The impact on sustainability of the topology optimization (TO) of the mold structure, i.e., steel support plate design (Figs. 6, 7, 12), is reported in [26,36]. The outcomes of these papers, mainly lightweighting obtained with the mechanical TO, were analyzed using LCA & LCC to

Table 7
Comparison of support plate weights.

Mold component	CM (g)	HM (g)	ΔW (−)	ΔW% (%)
Injection Support plate	634	80	−554	−87.4%
Ejection Support plate	620	68	−552	−89.0%

assess the impact on sustainability. In both papers, the conclusions state that, compared to Conventional Mold (CM), the Topology Optimized Injection Mold (TOIM) shows an advantage in environmental impact over an extended lifespan, emphasizing the importance of a life cycle assessment. The Cumulative Energy Demand (CED) analysis shows that TOIM becomes advantageous at a Sustainable Break-Even Point (S-BEP) of 68.5% of the mold's lifespan. In End-of-Life (EoL) efficiency analysis, recycling scenarios reveal that both TOIM and CM benefit from high material recovery rates. However, TOIM demonstrates potential to further reduce impact through improved recycling strategies. The assessments of Global Warming Potential (GWP) and endpoint damage to human health and ecosystems were also reported in [26].

The LCA & LCC of mold's support plates made of different materials: stainless steel, aluminum alloys, high-performance polymers (i.e., PEEK), and the photopolymer resin HT used in this work, with a topologically optimized design, is reported in [37]. This paper investigates the effects on some sustainability parameters of the different manufacturing process chains, materials, and their performance, weight reduction, cost structures, etc. Outcomes are analyzed with a global assessment and a sensitivity analysis. The paper's conclusion refers to a mass reduction of up to 22%, which results in cost and environmental savings of 30–45% during the production and use phases. Although with a potential 50% reduction in service life for polymeric materials (PEEK and HT resin). A complete comparison (sensitivity analysis) of the four solutions is also presented, with a clear identification of advantages and disadvantages. The mold with components made of PEEK or photopolymer resin HT was reported to have the best performance in terms of lightweighting design and environmental performance. All these studies address the analysis of lightweight molds, mold manufacturing, the use phase (injection molding) throughout the mold life span, and the energy demand of injection molding machines. Further studies are underway to measure and assess the effects of energy efficiency, particularly thermal energy management, on the industrial sustainability of the innovative mold presented in this work.

6. Conclusions

This study proposes an innovative hybrid mold design for injection molding, combining steel inserts with polymeric/composite support plates to enhance thermal energy management. The results show that the hybrid configuration significantly alters the thermal behavior of the mold, leading to higher heat retention within the inserts (up to approximately 30 °C increase compared to the conventional mold), faster thermal transients, and reduced heat dissipation to the environment. The numerical model demonstrated good predictive capability, with temperature deviations generally below 5 °C when compared with experimental measurements under different operating conditions. This confirms the robustness of the proposed modeling approach in capturing the main thermal phenomena of the process. The numerical energy analysis highlights a clear benefit of the hybrid solution, with a 4% increase in energy retention per cycle and a cumulative gain of 55% during the warm-up phase. A significant weight reduction of about −88% in the mold support plate was also achieved with the polymer and an optimized design. In addition, while heat accumulation is traditionally considered a drawback, this work demonstrates that it can be effectively exploited when combined with efficient heat extraction strategies, enabling potential energy recovery and reuse. Future developments will focus on integrating conformal cooling solutions, increasing mold durability, industrial sustainability assessment, and extending the approach to larger-scale applications, where potential energy savings are expected to be even more significant.

CRediT authorship contribution statement

Vito BASILE: Writing – review & editing, Writing – original draft, Validation, Supervision, Project administration, Methodology, Investigation, Funding acquisition, Data curation, Conceptualization. **Giulia ZANIBONI:** Writing – original draft, Visualization, Validation, Software, Resources, Data curation. **Riccardo PELACCIA:** Writing – original draft, Visualization, Validation, Software, Methodology, Investigation, Data curation. **Rossella SURACE:** Writing – original draft, Resources, Investigation, Data curation. **Leonardo ORAZI:** Writing – review & editing, Supervision, Resources, Project administration, Funding acquisition, Formal analysis. **Francesco Giovanni MODICA:** Writing – review & editing, Validation, Resources, Data curation. **Irene FASSI:** Writing – review & editing, Supervision, Resources.

Fundings

This work was funded by the European Union under the Italian National Recovery and Resilience Plan (NRRP) of NextGenerationEU, partnership on “Next generation of sustainable and highly efficient molding processes” Italian Projects of Significant National Interest (PRIN) PNRR 2022 grant n. P2022ZE23N.

Declaration of competing interest

The authors declare the following financial interests/personal relationships which may be considered as potential competing interests: Vito Basile reports financial support was provided by European Commission. If there are other authors, they declare that they have no known competing financial interests or personal relationships that could have appeared to influence the work reported in this paper.

Acknowledgements

The authors gratefully acknowledge the technical support of Mr. Elia Andretto (CNR-STIIMA) during the manufacturing phases of the research.

Appendix A. Supplementary data

Supplementary data to this article can be found online at https://doi.org/10.1016/j.jmapro.2026.09.033.

References

[1] Fu H, Xu H, Liu Y, Yang Z, Kormakov S, Wu D, et al. Overview of Injection Molding Technology for Processing Polymers and Their Composites. ES Materials & Manufacturing 2020;8(2020):3–23.
[2] Czepiel Mateusz, Bańkosz Magdalena, Sobczak-Kupiec Agnieszka. Advanced injection molding methods. Materials 2023;16(17):5802.
[3] Radu I-C, Vadureanu A-M, Cozorici D-E, Blanzeanu E, Zaharia C. Advancing Sustainability in Modern Polymer Processing: Strategies for Waste Resource Recovery and Circular Economy Integration. Polymers (Basel) 2025;17:522. https://doi.org/10.3390/polym17040522.
[4] Lucchetta G, Masato D, Sorgato M. Optimization of mold thermal control for minimum energy consumption in injection molding of polypropylene parts. J Clean Prod 2018;182:217–26. https://doi.org/10.1016/j.jclepro.2018.01.258.
[5] Smith AG, Wrobel LC, McCalla BA, Allan PS, Hornsby PR. A computational model for the cooling phase of injection moulding. J Mater Process Technol 2008;195:305–13. https://doi.org/10.1016/j.jmatprotec.2007.05.018.
[6] Rashid Oliver, Low KWQ, Pittman JFT. Mold cooling in thermoplastics injection molding: Effectiveness and energy efficiency. J Clean Prod 2020;264:121375.
[7] Silva HM. A review of the design optimization of conformal cooling channels in injection molds. Int J Adv Manuf Technol 2025. https://doi.org/10.1007/s00170-025-15234-2.
[8] Qi X, Li J, Liang Y, Xu Z, Li Y, Xie Z. Optimization of Mold Heating Structure Parameters Based on Cavity Surface Temperature Uniformity and Thermal Response Rates. Polymers 2025;17:184. https://doi.org/10.3390/polym17020184.
[9] Su Quanliang, Zhang Nan, Gilchrist Michael D. The use of variotherm systems for microinjection molding. J Appl Polym Sci 2016;133:9.
[10] Altaf K, Rani A Majdi Abdul, Raghavan VR. Prototype production and experimental analysis for circular and profiled conformal cooling channels in aluminium filled epoxy injection mould tools. Rapid Prototyp J 2013;19:220–9. https://doi.org/10.1108/13552541311323236.

[11] Au KM, Yu KM. A scaffolding architecture for conformal cooling design in rapid plastic injection moulding. Int J Adv Manuf Technol 2007;34:496–515. https://doi.org/10.1007/s00170-006-0628-x.
[12] Vetter J, Beneder S, Schmidt M. Material-tailored tool inserts for injection moulding using material extrusion multi-material Additive Manufacturing. Procedia CIRP 2024;124:231–4. https://doi.org/10.1016/j.procir.2024.08.106.
[13] de Souza Marconi PGC, Beal VE, Ferreira CV, et al. Systematic approach for injection mold rapid tooling. Int J Adv Manuf Technol 2025. https://doi.org/10.1007/s00170-025-17024-2.
[14] Kuo Chil-Chyuan, Farooqui Armaan, Tasi Cheng-Xuan, Pan Xin-Yu, Huang Song-Hua. Revolutionizing metal powder injection molding: A cost-effective approach to tooling innovation. J Manuf Process 2025;150:900–13.
[15] Kuo Chil-Chyuan, Lin Pin-Han, Jing-Yan Xu, Lin Zhe-Xhi, Wang Zi-Huan, Huang Song-Hua. Polymeric advancements in innovating wax injection molds using aluminum-filled epoxy resin with face-cooled waterfall cooling channels. J Manuf Process 2024;124:954–65.
[16] Kolbe C. Strahlschmelzen - LaserCUSING® - Integration im Werkzeug- und Formenbau. RTe J. 2010;7(1):1–7. https://rtejournal.de/rte/article/view/2010_3. [Accessed 7 March 2025].
[17] Berger GR, Zorn D, Friesenbichler W, Bevc F, Bodor CJ. Efficient cooling of hot spots in injection molding. A biomimetic cooling channel versus a heat-conductive mold material and a heat conductive plastics, Polymer Engineering & Science 2019;59:E180–8. https://doi.org/10.1002/pen.25024.
[18] Silva HM, Noversa JT, Fernandes L, Rodrigues HL, Pontes AJ. Design, simulation and optimization of conformal cooling channels in injection molds: a review. Int J Adv Manuf Technol 2022;120:4291–305. https://doi.org/10.1007/s00170-022-08693-4.
[19] Arman S, Lazoglu I. A comprehensive review of injection mold cooling by using conformal cooling channels and thermally enhanced molds. Int J Adv Manuf Technol 2023;127:2035–106. https://doi.org/10.1007/s00170-023-11593-w.
[20] Basile V, Modica F, Surace R, Fassi I. Micro-texturing of molds via Stereolithography for the fabrication of medical components. Procedia CIRP 2022;110:93–8. https://doi.org/10.1016/j.procir.2022.06.019.
[21] Surace Rossella, et al. Micro injection molding of thin cavities using stereolithography for mold fabrication. Polymers 2021;13(11):1848. https://www.mdpi.com/2073-4360/13/11/1848.
[22] Moritz VF, Bezerra GSN, Hopkins Jnr M, Fuenmayor E, Günbay S, Hayes C, et al. Heat Dissipation Plays Critical Role for Longevity of Polymer-Based 3D-Printed Inserts for Plastics Injection Moulding. J Manuf Mater Proc 2022;6:117. https://doi.org/10.3390/jmmp6050117.
[23] Park SJ, Lee JH, Yang J, Heogh W, Kang D, Yeon SM, et al. Lightweight injection mold using additively manufactured Ti-6Al-4V lattice structures. J Manuf Process 2022;79:759–66. https://doi.org/10.1016/j.jmapro.2022.05.022.
[24] Bellantone V, Surace R, Trotta G, Fassi I. Replication capability of micro injection moulding process for polymeric parts manufacturing. Int J Adv Manuf Technol 2013;67:1407–21. https://doi.org/10.1007/s00170-012-4577-2.
[25] High Temp resin technical datasheet. 2020. Available at: https://media.formlabs.com/m/41c07afd78a70b19/original/-ENUS-High-Temp-TDS.pdf (accessed on November 2025).
[26] Serratore G, Borda F, Basile V, Filice L. Life cycle assessment-guided design for sustainable microinjection molds. Materials Research Proceedings 2025;54:1807–16. https://doi.org/10.21741/9781644903599-194.
[27] Modica Francesco, Basile Vito, Fassi Irene. An experiment-based variable compensation method to improve the geometric accuracy of sub-mm features fabricated by stereolithography (SLA). J Manuf Mater Proc 2024;8(3):90.
[28] Basile Vito, Modica Francesco, Fassi Irene. Software compensation to improve the Stereolithography fabrication of porous features and porous surface texturing at micro-scale. Procedia Computer Science 2024;232:2072–81.
[29] Basile Vito, et al. Process chains for micro-manufacturing: modeling and case studies. J Manuf Mater Proc 2023;7(6):215.
[30] Burlaga B, Kroma A, Poszwa P, Kłosowiak R, Popielarski P, Stręk T. Heat Transfer Analysis of 3D Printed Wax Injection Mold Used in Investment Casting. Materials 2022;15:6545. https://doi.org/10.3390/ma15196545.
[31] Lodygowski T, Rakowski J, Litewka P. Recent Advances in Computational Mechanics. CRC Press; 2014.
[32] Wagner G, Nóbrega JM. Conformal Cooling Channels in Injection Molding and Heat Transfer Performance Analysis Through CFD—A Review. Energies 2025;18:1972. https://doi.org/10.3390/en18081972.
[33] Oubellaouch K, Pelaccia R, Orazi L, et al. A novel experimental-numerical procedure for the rheological characterization of thermoplastic polymers applied to injection molding. Int J Adv Manuf Technol 2025;140:5419–33.
[34] CAMPUS®. Material information system for the plastics industry. 2026. Available at: https://www.campusplastics.com/ (Accessed on September 2026).
[35] Park Hyung-Pil, et al. A Study on the Void Formation in Residual Wall Thickness of Fluid-assisted Injection Molding Parts. Adv Mater Sci Eng 2014;2014(1):238251.
[36] Borda F, Basile V, Gagliardi F, Filice L. Life Cycle Costing of new generation of molds for microinjection molding process. Procedia Computer Science 2026;277:1433–42. https://doi.org/10.1016/j.procs.2026.02.182.
[37] Borda F, Basile V, Gagliardi F, Filice L. Sustainability-Driven Business Model in Mold Manufacturing: A Multi-Criteria Comparison between Conventional and Additive Technologies. Key Eng Mater 2026;1051:61–71. https://doi.org/10.4028/p-9JSPCw.